Inhibition of Ral GTPases using a stapled peptide approach

Jemima C. Thomas[1,2,4], Jonathan M. Cooper[3], Natasha S. Clayton[1], Chensu Wang[3], Michael A. White[3], Chris Abell[2], Darerca Owen[1*] and Helen R. Mott[1*]

[1]Department of Biochemistry, University of Cambridge, Cambridge, CB2 1GA, UK
[2]Department of Chemistry, University of Cambridge, Cambridge, CB2 1EW, UK
[3]Department of Cell Biology, UT Southwestern Medical Center, Dallas, TX 75390-9039, USA
[4]Current address: Institute of Cancer Research, 15 Cotswold Road, Sutton, SM2 5NG, UK

*To whom correspondence should be addressed: Dr Helen R. Mott or Dr Darerca Owen, Department of Biochemistry, 80, Tennis Court Road, Cambridge CB2 1GA. Telephone: (01223) 764825; FAX: (01223) 766002; Email: do202@cam.ac.uk (DO), hrm28@cam.ac.uk (HRM)

Running title: Inhibition of Ral GTPases using stapled peptides

ABSTRACT

Aberrant Ras signalling drives numerous cancers and drugs to inhibit this are urgently required. This compelling clinical need, combined with recent innovations in drug discovery including the advent of biologic therapeutic agents, has propelled Ras back to the forefront of targeting efforts. Activated Ras has proved extremely difficult to target directly and the focus has moved to the main downstream Ras-signalling pathways. In particular, the Ras-Raf and Ras-PI3K pathways have provided conspicuous enzyme therapeutic targets, which were more accessible to conventional drug-discovery strategies. The Ras-RalGEF-Ral pathway is a more difficult challenge for traditional medicinal development and there have therefore been few inhibitors reported that disrupt this axis. We have used our structure of a Ral-effector complex as a basis for the design and characterization of α-helical stapled peptides that bind selectively to active, GTP-bound Ral proteins and that compete with downstream effector proteins. The peptides have been thoroughly characterized biophysically. Crucially, the lead peptide enters cells and is biologically active, inhibiting isoform-specific RalB-driven cellular processes. This therefore provides a starting point for therapeutic inhibition of the Ras-RalGEF-Ral pathway.

Ras is well-established as the most frequently mutated oncogene in human cancer. This small G-protein cycles between an active GTP-bound state and an inactive GDP-bound state. Molecular switching between the 'on' and 'off' states is positively regulated by nucleotide guanine exchange factors (GEFs)[1] and negatively regulated by GTPase-activating proteins (GAPs). It is only the active, GTP-bound form of the protein that can bind to downstream effectors and facilitate signal transduction. Mutations in oncogenic Ras result in a constitutively active protein that remains fixed in the GTP-bound 'on' state, leading to unregulated activation of downstream pathways. These mutations are found in approximately 30% of all cancers, with a higher occurrence in specific cancer types such as pancreatic (71%) and colorectal (45%) (1). This makes Ras a crucial cancer therapeutic target; nevertheless, Ras has so far evaded direct attempts at inhibition and many Ras-driven cancers are currently deemed undruggable. Ras signalling has proven difficult to disrupt by small, drug-like molecules because its activation of downstream cascades is accomplished through protein-protein interactions, which have traditionally been avoided as drug targets due to the large, shallow surfaces involved in protein-protein interfaces (2-4). Likewise, there are no obvious clefts or small molecule binding pockets on Ras and competitive inhibition with the nucleotide is unfeasible due to the extremely high affinity of GTP binding and its high concentration

1

in the cellular environment (5,6). Logical attempts to interfere with critical post-translational modifications of Ras, such as inhibition of farnesyltransferase, have also proved unsuccessful (reviewed in (1,6,7)). More encouragingly, a specific Ras variant found in lung cancer, G12C, was successfully used in a recent disulphide fragment-based screen to identify small molecules that covalently modify this precise Ras mutant (8). This led to the identification of a potential allosteric site that may be targetable in this particular mutant. The problems with attacking Ras directly have driven a broader search for drug targets that will interfere with Ras signalling, with a focus on the effector proteins downstream of Ras (reviewed in (1,6)). Following Ras activation there are several pathways that propagate the cellular signal, of which at least five have been implicated in oncogenic signalling (9). Of these, the Raf, phosphoinositide 3-kinase (PI3K) and RalGEF are the best validated (6). Both Raf and PI3K have been the object of several drug discovery initiatives in recent years, with inhibitors of both proteins currently in clinical trials (10,11). However, the third pathway, via RalGEFs, has been less extensively studied and no therapies exist that disrupt this signalling route. Despite this, RalA and RalB have been shown to be important drivers of cell growth, cell survival and metastasis in many human cancers, including bladder, melanoma, colorectal and pancreatic (12,13).

RalGEFs act to activate RalA and RalB, themselves small GTPases of the Ras superfamily. Like Ras, the Ral proteins cycle between GTP and GDP-dependent 'on' and 'off' states and are involved in regulating diverse cellular processes including proliferation, motility and maintenance of cellular architecture (13). RalA and RalB are 206 amino acid proteins that are 82% identical, with 100% identity in the nucleotide-sensitive switch regions (switch 1 and switch 2). Intriguingly both GTP-loaded proteins interact directly with the same set of downstream effectors *in vitro*, including RLIP76 (or RalBP1), the exocyst complex subunits Sec5 and Exo84 and the transcription factor ZO-1-associated nucleic-acid-binding protein (ZONAB) (12). Despite engaging the same collection of effector proteins, RalA and RalB nevertheless regulate distinct cellular functions and play different roles in

tumourigenesis. This is partly attributable to the ability of the effectors themselves to promote multiple signalling pathways. For example, both Ral isoforms interact with Sec5, which can act as an integral member of the exocyst complex, controlling exocytosis (14,15), but RalB-Sec5 can also engage and activate TBK1 and contribute to cancer cell survival (16). Interestingly, although RalA and RalB have similar affinities for the effectors that have been tested *in vitro* (17-19), they may actually possess different affinities *in vivo* (20), explaining some of their distinct cellular functions. Some differences between RalA and RalB will be due to the hypervariable C-terminal region of the proteins, which is differentially phosphorylated (21-23) and ubiquitinated (24), resulting in distinctive and specific subcellular localization for the two proteins. Differential activation and deactivation by the RalGEF and RalGAP family may also contribute to differential roles for the two Ral isoforms. However, no GEFs have been found that discriminate between the two Ral isoforms and the one structure of a RalGEF with Ral shows that all the contacts with the GEF protein are conserved between RalA and RalB (25) Similarly, RalGAPs appear to act on both isoforms *in vitro* (26) and in cell lines (27).

Several studies have been reported that attempt to delineate separate cellular roles for RalA and RalB. siRNA inhibition experiments showed that knockdown of RalB in HeLa, MCF7 and SW480 cell lines resulted in apoptosis, with no effect observed in non-cancerous human cell lines, suggesting that tumour cells may become dependent on RalB survival pathways (28). Inhibition of RalA in these experiments had no effect on adherent cells but impaired anchorage-independent proliferation of cells in suspension. In contrast, Lim *et al*. (29) found that RalA, but not RalB, was required for oncogenic transformation of human fibroblasts and HEK-HT cells and is critical for Ras-driven tumourigenesis. Similar effects have been observed in human pancreatic cancer and colorectal cancer cell lines and, interestingly, RalB appears to be important during cell invasion and metastasis of these cancers (30,31). The molecular basis of the divergent functions of RalA and RalB in both normal and malignant cells remains to be elucidated. It is clear however that both proteins play key roles in

2

tumourigenesis and cancer progression and are therefore potential therapeutic targets.

The Ral proteins adopt the same overall structural fold as Ras and are therefore equally difficult to disrupt using small molecules. Small molecules that bind to inactive, GDP-bound forms of Ral have, however, recently been identified using *in silico* screens (32). Our solution structure of RalB·GMPPNP in complex with the Ral-binding domain of RLIP76 (RLIP76 RBD) (33) showed novel features for a Ras family-effector complex and presented an avenue for structure-guided design of inhibitors that would target the active, GTP-bound form of the Ral proteins. The GTP-bound form is generated downstream of activated Ras, so such inhibitors would bind specifically to chronically activated Ral, as would be encountered in the disease context. The structures that are currently available reveal that most Ras and Ral effectors form intermolecular β-sheets with the small G protein or interact through loops and unstructured regions (34). In stark contrast, the RLIP76 RBD adopts a well-structured coiled-coil domain, consisting of two α-helices that do not significantly change conformation on Ral complex formation (33). Mimicry of these helices offers an ideal opportunity to simulate effector binding and inhibit Ral-effector interactions, stopping signalling from Ral proteins and ultimately from Ras. Biological validation of this proposition has already been reported with the observation that overexpression of the RLIP76 RBD can interfere with Ral signalling, leading to mislocalization of Ral-interacting proteins and prevention of RalA-dependent anchorage-independent growth (14,28,35).

In a timely confluence, the mimicry and stabilization of α-helices has been an emerging area in inhibitor design in recent years, particularly through the use of chemically 'stapled' peptides. The introduction of a staple confers multiple, advantageous, drug-like qualities on the peptides: the staple stabilizes the α-helical conformation of small peptides leading to an increase in binding affinity, it improves the cell penetrating ability of the peptide and it enhances the resistance of the peptide to protease degradation. This technique has been successfully applied to several different protein targets (36,37) and the first stapled peptide

based therapy, a long acting growth hormone releasing hormone (GHRH) agonist, has passed Phase I clinical trials, while the first anti-cancer stapled peptide, targeting the reactivation of p53, has also now entered Phase I trials (38). Peptides based on a helix from the Ras exchange factor SOS have been used to target Ras (39,40), suggesting that small G proteins are amenable to such approaches. The Ras-binding peptides designed so far are not selective for the GTP-bound form of the Ras protein, although the stapled versions bind with a high affinity to wild-type K-Ras and several oncogenic mutants (40).

Here, we report the design and characterization of peptides based on a single helix of the RLIP76 RBD that bind selectively to active, GTP-bound Ral. This work provides proof of principle that a single helix of RLIP76 is responsible for the majority of the RLIP76 interactions with Ral and that it is possible to use this approach to obtain peptides specific to the active form of a small GTPase. We describe stapled peptides based on this helix that have cell-penetrating ability and are biologically active. These peptides provide the basis for further maturation to therapeutically useful antagonists of Ral and Ras signalling.

Results

A peptide based on RLIP76 RBD α2 is sufficient to bind RalA and RalB.

Our previously reported NMR solution structure of the Ral-binding domain (RBD) of RLIP76 bound to active, GMPPNP-loaded, RalB (33) showed that RLIP76 employs a coiled-coil motif to bind to Ral. The structure suggested that most of the key interactions with Ral are mediated by the C-terminal helix (hereafter α2) of the RLIP76 RBD coiled-coil (Figure 1a). Indeed, 80% of the buried surface area in the complex involves helix α2 and alanine scanning mutagenesis identified more energetic hotspots within this helix than in α1 (the N-terminal helix of the coiled-coil) (17). To determine whether helix α2 is sufficient for binding to RalB, we synthesized two separate peptides based on the contact surfaces in helix α1 and α2. Peptide 1 comprised the full helix α2 sequence, residues 423-446, to encompass all of

the RalB-interacting residues in this helix. Peptide 2 incorporated residues 408-422 and comprises residues corresponding to the last two turns of helix α1 together with the short loop that connects α1 and α2. This peptide therefore includes all the contacts to RalB outside helix α2.

Circular dichroism (CD) spectroscopy experiments performed on the complete RLIP76 RBD resulted in a characteristic α-helical spectrum with minima at 208 and 222 nm (Figure 1b). The helical content calculated from the CD spectra was 77% (Figure 1c), in agreement with the 78% seen in the structure of free RLIP76 RBD ((33), pdb code: 2kwh). CD analysis of the two synthetic peptides revealed that Peptide 1 was 50% helical in solution, while Peptide 2 was only 4% helical (Figure 1b,c). The helical content of the residues equivalent to Peptides 1 and 2 in the context of the entire RBD is 96% and 53% respectively. Therefore the helices in both peptides are destabilized when they are not in the context of the coiled-coil. Peptide 1 however, clearly retains some helical propensity in isolation, and presumably is in equilibrium between structured and unstructured states. Conversely, Peptide 2 shows little propensity to form any helix when it is removed from the coiled-coil, and its CD spectrum is characteristic of a random coil (Figure 1b).

The binding of the RLIP76 RBD, Peptide 1 and Peptide 2 to RalB was investigated using isothermal titration calorimetry (ITC). The RLIP76 RBD coiled-coil bound to RalB with an affinity of 1.9 μM (Figure 2a, Table 1) and with a similar affinity (4.6 μM) to RalA•GMPPNP (data not shown). The interaction appears to be driven by a relatively large, favourable enthalpic term, which counteracts the unfavourable entropy loss that occurs when the two domains come together. Peptide 1 also bound to RalB but with a lower affinity. The K_d was around 30 μM, an order of magnitude weaker than the full coiled-coil domain of RLIP76 RBD (Figure 2b, Table 1). In contrast, Peptide 2 showed no heat changes when titrated into RalB under the same conditions, supporting the idea that most Ral binding contacts occur through RLIP76 RBD α2, (Figure 2c). Encouragingly, while ITC showed that Peptide 1 also bound to RalA, with K_d 43 μM (Figure 2d, Table 1), it showed no interaction with the Rho-

family GTPase Rac1 (Figure 2e), indicating that binding of this single helix is selective for Ral small G proteins.

The ITC data for Peptide 1 revealed that when this peptide binds to RalA and RalB the ΔS term is positive, in contrast to the entropy loss that was observed when RLIP76 RBD and Ral proteins interact. This favourable entropy change increases the binding affinity, which would otherwise be drastically reduced by the smaller enthalpic gain when the peptides bind (Table 1).

A peptide based on RLIP76 RBD α2 binds to RalB on the same interface as RLIP76.

Given the altered thermodynamics of the interaction, it is possible that Peptide 1 binds to a different region of the Ral proteins. To ascertain whether Peptide 1 binds in a similar manner as the RLIP76 RBD, ^{1}H-^{15}N HSQC NMR experiments were used to map the binding surface on RalB utilized by Peptide 1. HSQC spectra of uniformly ^{15}N-labelled RalB·GMPPNP were recorded both alone and in the presence of increasing amounts of Peptide 1. Addition of Peptide 1 caused several RalB peaks to shift and in some cases to lose intensity (Figure 3a), which is consistent with a mixture of fast and intermediate exchange on the NMR timescale. This is likely to be due to the switch regions of RalB undergoing conformational exchange when in the complex with the peptide. A titration was performed at a range of RalB:Peptide 1 ratios from 1:0 to 1:8, which, along with the previously reported backbone assignment (41), allowed most of the crosspeak positions to be tracked. The majority of the peaks in the peptide complex were assigned and their positions compared with those of the peaks corresponding to the same residues in the RalB-RLIP76 RBD complex. Comparison of the HSQC spectra of free RalB·GMPPNP with RalB·GMPPNP-Peptide 1 and RalB·GMPPNP-RLIP76 RBD shows that those peaks that shifted tended to move in the same direction in both complex spectra (Figure 3a). For example, Arg52, which experienced a relatively large shift, moved in the Peptide 1 complex to a position very close to that of the Arg52 crosspeak in the RLIP76 RBD complex. The peak positions in free RalB·GMPPNP and in RalB·GMPPNP-Peptide 1 were used to calculate the overall chemical shift change (Figure 3b). The

4

changes are concentrated in the N-terminal half of the RalB protein, which includes the two nucleotide-sensitive switch regions. The residues that experienced a significant shift change (larger than the standard deviation of all changes) were mapped onto the RalB structure (Figure 3c). These included several residues that are unlikely to be directly contacting Peptide 1, because they are buried in the free RalB structure (42). These shift changes, which also occurred when the RLIP76 RBD was titrated into RalB, are indicative of subtle conformational rearrangements that are often observed when small G proteins such as RalB bind to their effectors (DO and HRM, unpublished observations). The solvent accessibility of the RalB·GMPPNP residues was assessed using NACCESS (43). Residues that are shifted, and are at least 50% solvent exposed, are highlighted in Figure 3c. All of these residues are within, or close to, the switch regions and most of them are in direct contact with the C-terminal helix of RLIP76 RBD in the complex (Figure 3c,d). Two residues that shift but do not contact RLIP76 are Val40[RalB] and Glu41[RalB]. These are at the beginning of switch 1, while Asp49[RalB] at the opposite end of the same switch is in direct contact. The structure and dynamics of the whole switch region changes in the RLIP76 complex and the chemical shifts of Val40 and Glu41 are likely to be sensitive to this. The crosspeaks for most of switch 1 are not visible in the spectra of free RalB·GMPPNP, so it is not possible to see changes for other residues within the same loop. Overall, the correlation between crosspeak positions in the RalB·GMPPNP-Peptide 1 and RalB·GMPPNP-RLIP76 RBD spectra, along with the positions of the residues that exhibit the largest chemical shift changes indicate that the contact surface for Peptide 1 on RalB is identical to that of the RLIP76 RBD helix α2.

Design and synthesis of RLIP76-based stapled peptides

Having established that an RLIP76 RBD-based α2 peptide could selectively bind to Ral in an analogous manner to the RLIP76 RBD, we sought to improve its binding affinity. Chemical stapling of peptides has been shown to increase their helicity and often enhances their binding to target proteins (36). Stapled peptides were synthesized using a well-established solid-phase peptide synthesis method for incorporation of all-hydrocarbon staples (44). Two unnatural amino acids containing α-methyl, α-alkenyl side-chains were introduced into the peptide sequence, and the staple covalently formed by ruthenium-catalysed ring-closing metathesis (Figure 1a,c). Five stapled peptides were designed based on RLIP76 RBD α2 (SP1-SP5), as Peptide 1 had already been confirmed to bind Ral. One stapled peptide was also designed based on RLIP76 RBD helix α1 (SP6) to investigate whether increased secondary structure in Peptide 2 could facilitate Ral complex formation. Examination of the RalB·GMPPNP-RLIP76 RBD structure (33), together with computational and experimental alanine scanning mutagenesis data (17) revealed those RLIP76 RBD residues that were the most important for Ral binding (Figure 1a). These included three residues in helix α1 (Leu409, His413 and Leu416) and five residues in helix α2 (Leu429, Trp430, Arg434, Thr437 and Lys440). Individual mutation of any of these residues to Ala reduced the binding affinity of RLIP76 RBD for RalA or RalB more than 5-fold (17). These vital binding residues were retained in the peptide sequences and the chemical staples were positioned on the opposite face of the α-helix to allow these key residues to drive complex formation (Figure 1a,c). Peptides were synthesized with different staple lengths and staple positions to enable screening for optimum binding. SP1, SP2 and SP3 contained a single *i*, *i*+4 staple, which was placed in various positions along the α2 helix. SP6, based on helix α1 and the interhelix loop, only included three turns of α-helix. This peptide also contained a single *i*, *i*+4 staple, however only a single staple position was tested, as other positions would potentially disrupt the structure of the loop. SP4 and SP5 were also based on helix α2: SP4 contained one *i*, *i*+7 staple, and SP5 was doubly stapled, with two *i*, *i*+4 linkages (Figure 1c). All peptides were acetylated at the N-terminus and included a C-terminal amide bond. Following purification, the helicity of the stapled peptides was determined by CD spectroscopy (Figure 1b,c). Incorporation of the staples increased the helicity of most of the RLIP76 RBD peptides compared to their unstapled counterparts: SP1, SP3, SP4 and SP5 showed extremely high helicity (80-90%), much more than the unstapled Peptide 1, and close

to the ~90% expected if the peptides were to adopt the same structure as α2. SP2 was the least helical of the α2-based stapled peptides, and had the same helicity as the unstapled Peptide 1, suggesting that the staple at this position does little to stabilize the helix. Stapling of the unstructured Peptide 2 also significantly increased its helicity, although SP6 was still only 57% α-helical, less than the ~75% expected if the peptide had the same structure as the equivalent sequence in the RLIP76 RBD.

SP1 binds to RalB with increased affinity compared to unstapled Peptide 1.

Stapled peptide binding to RalB·GMPPNP was investigated using ITC, as for the unstapled peptides (Figure 4). All of the stapled peptides based on the RLIP76 RBD α2 sequence (SP1-SP5) were able to bind RalB but the stapled analogue of α1, SP6, did not exhibit any heat changes, despite its increased helicity. This suggests that the binding interactions made between RLIP76 RBD α1 and RalB are not strong enough to enable complex formation in the absence of the α2 helix. The α2-based peptides SP3, SP4 and SP5 bound RalB with K_d 16-53 μM (Table 1), which are similar to the affinity of the unstapled Peptide 1 (30 μM). Compared with Peptide 1, SP1 and SP2 displayed enhanced affinity, with K_d values 4.7 μM and 10.3 μM respectively.

The binding of the stapled peptides was characterized by similar ΔH terms (of the order of 1 kcal/mol), implying that the nature of the interfaces may be similar (Figure 4, Table 1). The exception was SP4, which has the longer, *i*, *i*+7 staple, and was characterized by very small heat changes and non-reproducible data in the ITC experiments. This implies that SP4 binds using predominantly hydrophobic interactions and therefore may not utilize the same binding mode as the other peptides. Similarly, SP5, which has a double staple, bound weakly, and the data could not be accurately fitted. The stapled peptides had more favourable entropy of binding compared with the unstapled Peptide 1, and the enhanced binding of SP1 and SP2 is entirely due to the increase in ΔS.

SP1 is selective for active Ral and binds competitively with Ral effector proteins

As SP1 bound to RalB with the highest affinity, this peptide was taken forward for further investigation. N-terminally fluorescein labelled, FITC-SP1 and FITC-Peptide 1, were synthesized for fluorescence polarization (FP) assays. The use of an orthogonal assay to measure peptide binding was also useful to validate the results obtained with ITC. Direct binding FP assays showed that SP1 bound RalB with a K_d value of 5.6 μM, similar to that measured by ITC (Figure 5a). The binding of Peptide 1 measured by FP was too weak to obtain an accurate fit (Figure 5b), which placed the K_d at ≥ 50 μM, in line with the value measured by ITC (Table 1). We also tested the binding of FITC-SP1 to RalA·GMPPNP and found that it bound but with a slightly lower affinity than to RalB·GMPPNP, with a K_d of 14.2 μM (Figure 5c). This is in agreement with the lower affinities that we observed when unstapled Peptide 1 or the RLIP76 RBD were titrated into RalA·GMPPNP in ITC experiments.

To investigate the specificity of SP1 for Ral proteins, we examined its ability to bind to R-Ras, which is another small G protein in the Ras-family. This is a stringent test of specificity, since R-Ras and RalB are both in the Ras family, have a sequence homology of 64 %, and are conserved in the effector binding region (Figure 3d). FITC-SP1 bound to R-Ras·GMPPNP but with an affinity of 30 μM, 5-fold weaker than RalB (Figure 5a). The affinity of FITC-Peptide 1 for R-Ras·GMPPNP could not be determined accurately but again was weaker than that of Peptide1 for RalB·GMPPNP (Figure 5b).

Attempts were made to perform chemical shift mapping experiments with SP1 and ¹⁵N-labelled RalB·GMPPNP, analogous to those shown in Figure 3. It was however, not possible to find conditions in which both SP1 and RalB were stable at sufficiently high concentrations for NMR. As the peptides were designed based on helices from a Ral effector, and the NMR chemical shift mapping had suggested that Peptide 1 was binding close to the switch regions, we reasoned that the peptide binding should be nucleotide dependent. Nucleotide-dependent binding of SP1 to Ral would also imply that SP1 binds to Ral in the same

regions as Peptide 1. When RalA·GDP was titrated into FITC-SP1 (Figure 5c) no significant binding was observed, indicating that SP1 binding to Ral is dependent upon the GTP-bound conformation of the switch regions. Therefore, as is the case for GTPase effector proteins, SP1 preferentially binds active, GTP-bound Ral over the inactive, GDP-bound state.

To determine whether effector proteins could compete with SP1 for binding to RalB, a competition FP assay was performed. Increasing amounts of the RLIP76 RBD were titrated into a pre-formed complex of RalB·GMPPNP-FITC-SP1. The resulting decrease in FP signal (Figure 5d) indicates that FITC-SP1 and the RLIP76 RBD bind competitively to RalB·GMPPNP. The RLIP76 RBD was able to fully displace FITC-SP1 with an IC_{50} of 2.0 µM, which is comparable with the K_d for RalB·GMPPNP-RLIP76 RBD measured by ITC. This indicates that the peptide and RLIP76 RBD use the same interface to bind RalB·GMPPNP. We were interested in exploring whether other Ral effectors could also compete with SP1 for RalB·GMPPNP binding. The Sec5 RBD binds to Ral proteins with a higher affinity than RLIP76: both RalA and RalB bind Sec5 RBD with a K_d of ~100 nM (42). When the Sec5 RBD was titrated into the RalB·GMPPNP-FITC-SP1 complex, the FP signal was reduced. However, Sec5 did not cause complete loss of the FP signal even at high concentrations, and resulted in an IC_{50} of 8.2 µM, *i.e.* much higher than its K_d. This indicates that although there is some overlap in the binding sites of SP1 and Sec5 RBD, even at high Sec5 concentrations some binding remains between FITC-SP1 and RalB·GMPPNP. This can be explained by the observation that the RLIP76 RBD binds to both switch regions of RalB (33), whereas Sec5 RBD only contacts switch 1 (18). Therefore the Sec5 RBD binding to switch 1 is unable to displace SP1 completely, which can continue to contact switch 2 even in the presence of Sec5. Taken together, the evidence indicates that FITC-SP1 binds in an analogous manner to α2 of the RLIP76 RBD, which contacts both switch regions and cannot be fully displaced by the Sec5 RBD.

FITC-SP1 can enter mammalian cells

For stapled peptides to have experimental or therapeutic value they must be able to access their intracellular targets. To assess the cell penetrating properties of RLIP76 RBD-based peptides, we monitored the cellular uptake of FITC-Peptide 1 and FITC-SP1 using confocal microscopy. HEK293T cells were treated with 10 µM FITC-Peptide 1, FITC-SP1 or FITC alone, overnight at 37 °C and fixed with formaldehyde before imaging (Figure 6a,b). Consistent with previous studies on stapled peptides (36,37,45,46), robust penetration of SP1 into cells was observed. In contrast, uptake of FITC alone or the unconstrained FITC-Peptide 1 was not detectable in any cells. These data also indicate that the stapled peptide is stable for at least 16 hours. Single-cell images indicate that FITC-SP1 localizes throughout the cell, entering the nucleus as well as diffusing through the cytosol (Figure 6b). Encouragingly, the cells treated with FITC-SP1 were observed to be in a similar state of health and confluency as the control cells, suggesting that the peptide is not inherently toxic.

Once we had established cellular uptake of SP1 we wanted to confirm that the inhibition of Ral-effector interactions that we had already demonstrated *in vitro* for the stapled peptide were maintained in a cellular context. To judge this, we examined the ability of SP1 to inhibit co-immunoprecipitation of RalB with an effector protein. We incubated HEK293T cells in the presence or absence of SP1, immunoprecipitated endogenous RalB and immunoblotted for the presence of Sec5. SP6, the stapled helical peptide based on helix α1, which showed no heat changes in ITC experiments (Figure 4f), was used as a control. We used Sec5 to investigate whether SP1 acts as a pan-RalB inhibitor in cells with similar activity to that which we had already observed *in vitro*. Endogenous Sec5 was observed to co-immunoprecipitate with RalB in the absence of peptide (Figure 6c) but the interaction was almost completely inhibited by SP1, 24 hours after treatment. Interestingly, SP6 also appeared to attenuate the RalB-Sec5 interaction, although not as strongly as SP1. This suggests that even though it showed no heat changes in the ITC experiments, SP6 exhibits some low affinity binding to RalB.

We can therefore conclude that SP1 enters cells and once it is intracellular it retains the ability to inhibit RalB interactions with its downstream effector proteins.

SP1 can inhibit RalB-driven autophagosome assembly in cells

We next sought to examine whether SP1 retained the biological activity of the RLIP76 RBD and could interfere with Ral signalling in cells. Previous studies have demonstrated the involvement of RalB in nutrient deprivation-induced autophagosome assembly through its interaction with the downstream effector Exo84 (35). RalB is localized to nascent autophagosomes and is activated in response to nutrient deprivation. In its active conformation, RalB·GTP binds directly to its effector Exo84, inducing the assembly of catalytically active ULK1 and Beclin1-VPS34 complexes on the exocyst, which drive isolation membrane formation and maturation. Thus RalB signalling is necessary and sufficient to engage autophagy. In contrast, RalA has no involvement in the control of autophagy; so monitoring the effects of SP1 on autophagy specifically reveals the effects of its inhibition of RalB. Autophagosome assembly can be monitored through the loss of the marker LC3, which is first recruited to autophagosomes prior to its degradation in autophagolysosomes (Figure 7a,b). Exogenous expression of the RLIP76 RBD inhibits RalB-Exo84 complex formation and prevents autophagosome formation and maturation (35). To investigate whether SP1 had the same effect, HeLa cells stably expressing GFP-LC3 were treated with the cell-permeable SP1 for 24 hours and assayed for autophagosomal flux with quantitative microtiter plate-based assays. SP1 but not SP6 exposure resulted in dose-dependent inhibition of GFP-LC3 turnover that was not reversed by nutrient starvation, indicating robust inhibition of autophagosomal maturation at 20μM SP1 (Figure 7c). These observations imply that SP1 is able to penetrate cells and achieve a sufficiently high intracellular concentration to bind to RalB and inhibit its biological activity. To confirm that the effects observed were due to the interaction between SP1 and RalB, the localization of TFEB was evaluated. TFEB is a direct mTORC1 substrate that is sequestered in the cytosol under nutrient replete conditions (47,48).

Nutrient starvation results in mTORC1 inactivation and consequent translocation of TFEB to the nucleus where it induces adaptive gene expression programs. TFEB localization was unimpaired in SP1-treated cells (Figure 7d), demonstrating that the SP1-dependent inhibition of autophagosome maturation is unlikely to be through non-selective disruption of cellular responses to nutrient deprivation.

Discussion

The Ras signalling pathway has been proven to be a key driver of numerous cancers and is therefore a crucial anti-cancer drug discovery target. The difficulty in obtaining drug-like compounds that inhibit Ras itself has led to broader targeting of downstream Ras pathways, including the kinases Raf and PI3K. These efforts have been hampered by unexpected discoveries: the first class of Raf inhibitors turned out to activate the pathway in Ras-driven cancers (10), while MEK and PI3K inhibitors are also less efficacious due to the presence of feedback loops and poor tolerance (11). The third main Ras-driven signalling pathway activates the small GTPases RalA and RalB through the RalGEFs. Evidence indicates that this pathway is equally important in conveying signals from oncogenic Ras to drive tumourigenesis and is therefore a valuable therapeutic target (1). This signalling route has not been as extensively studied as the Raf and PI3K systems and does not exhibit as many conventionally exploitable targets. In fact until very recently there have not been any chemical inhibitors reported that act on this branch of the Ras cascade. Recently, a potential allosteric site was identified on RalA and used as the basis for a virtual small molecule screen. This generated hits that inhibit RalA and RalB by binding to the small G proteins in their GDP-bound form, locking them in their inactive conformation. These molecules have biological activity in cell lines and are also efficacious in mouse xenografts driven by K-Ras/Ral, demonstrating the utility of Ral inhibition for therapeutic gain and representing an exciting step forward in cancer therapeutics (32). Here, we have used our structure of the RalB-RLIP76 RBD complex to design and synthesize all-hydrocarbon stapled peptides that bind to both RalA and RalB

8

in the active, GTP-bound conformation and compete with their effector proteins.

We used ITC to determine the affinities and thermodynamics of binding of the peptides. Interestingly, we obtained a K_d of 1.9 μM for the RalB·GMPPNP-RLIP76 RBD complex by ITC, 10-fold higher than the K_d of 184 nM that we had previously determined by scintillation proximity assay (SPA) (33). There are several likely reasons for these differences. Firstly, different techniques used to determine affinities often yield different K_d values. This has been shown for other Ral-effector complexes, for example RalA·GMPPNP binding to Sec5 RBD had a K_d of 137 nM measured by ITC (18) but a K_d 10 nM by SPR (19)). We also found that Cdc42·GMPPNP binding to PAK gave lower affinities with ITC (K_d 150 nM) than SPA (K_d 10 nM) (49)). The difference in the RalB-RLIP76 RBD affinity may also be affected by the use of the nucleotide used in the different experiments. In the ITC experiments, RalB was bound to the nucleotide analogue GMPPNP, while SPA utilized ^{3}H-labelled GTP. All the peptides synthesized in this study were examined for binding by ITC, so their relative values can be compared. Furthermore, the affinities measured using FP for the peptides were similar to those obtained by ITC, allowing comparison between the affinities measured with these techniques.

We have shown that a peptide based on a single helix from RLIP76 (Peptide 1) is sufficient to bind Ral, albeit with approximately 14-fold weaker affinity than the full coiled-coil domain that comprises the RBD. NMR mapping indicates that Peptide 1 interacts with RalB at the same binding interface as RLIP76 RBD, so the reduction in affinity is due to the smaller peptide making fewer contacts with Ral, rather than to a different mode of binding. ITC was used to measure the affinities but it also yielded useful information about the thermodynamics of the interactions (Table 1). The interaction between RalB·GMPPNP and the full RLIP76 RBD is driven solely by a large negative ΔH, as the entropy change is in fact unfavourable. An analysis of the interactions between the two proteins suggests that the interface comprises a mixture of hydrogen bonds/salt bridges and hydrophobic interactions, which involve both α-helices of the RLIP76 RBD. Presumably the

hydrophobic interactions between the two proteins are not sufficiently numerous to offset the entropy loss on association. In contrast, when the peptides bind, the enthalpy term is reduced 10-fold or more (although it is still negative) but the entropy term is now positive (Table 1). Some of the change in enthalpy compared to the full RBD binding is likely to be due to the loss of the three hydrogen bonds involving helix α1 predicted from the structure: His413(Nε)-Tyr82(OH), Leu416(CO)-Asn81(Hδ), Gln417(Hε)-Asp74(CO), which are not present in the peptide complexes. The switch in the entropic term from negative in the full RBD to positive in the peptides is probably due to the larger number of exposed hydrophobic sidchains in the peptides, which lowers the entropy of the free peptides. The stapled peptides bind more tightly than the unstapled versions because the entropic term is even more favourable and apart from SP4 (which gave poor, non-reproducible data), ΔS is proportional to the affinity (Table 1). Peptide stapling reduces the entropic cost of the peptide folding upon binding by forcing the helix to be pre-formed. The subtle differences between the stapled peptides may be due to slight conformational differences when the staple position is moved. These could change the extent of burial of sidechains in the interface.

The helicity of the stapled peptides shows little obvious correlation with their affinities. The helical content of SP1, SP3, SP4 and SP5 is almost equivalent, while SP2, which has the second tightest binding, is no more helical than Peptide 1 (Figure 1c). The helical content estimated by CD is, however, the *average* in solution. It is reasonable to assume that Peptide 1 exists in an equilibrium between helical and unstructured, and that, as it is 50% helical, the two populations are approximately equal. Binding to RalB then pushes the equilibrium to the helical state. In SP2 on the other hand, the stapling ensures that the centre of the peptide is helical, so that at least part of the peptide is helical all of the time. This shorter helix would then act as a nucleation site for the formation of the remainder of the helix on binding. For peptides such as SP3, which exhibits high helicity but low affinity, we can speculate that the staple position has locked the sidechains into a position where they can no longer make favourable interactions with RalB. It is noteworthy

9

that SP3 and SP4, neither of which binds tightly, both have their staple positioned behind the Trp within the peptide. Mutation of Trp430 in the context of the RLIP76 RBD knocks out binding completely (17) and the structure shows that this residue makes extensive interactions with RalB (33). It is likely that the rigidity imposed by stapling across the back surface of this Trp restricts at least some of these interactions.

The most potent RLIP76 RBD α2-based stapled peptide (SP1) bound to RalB with a 5-fold increase in affinity over the unstapled peptide. Previously published studies on stapled peptides have reported affinity increases between 2- and 100-fold, depending on the protein target (36,37). The 5-fold increase noted here therefore, is rather a modest effect. However, in this case the native unstapled peptide is already significantly helical (unlike many other peptides) and has a reasonable affinity compared with that of the RLIP76 RBD. The final affinity of the best stapled peptide is only ~2.5-fold weaker than the complete progenitor domain, the RLIP76 RBD and, as such, SP1 provides an excellent starting point for further optimization. Interestingly, the small molecule inhibitors identified for Ral also have a K_d of approximately 5-8 μM and are still effective inhibitors in both cell culture and animal models (32). These low μM K_d values reflect the difficulty in designing chemical inhibitors for Ral proteins and highlight the importance of our peptide.

Constrained peptides have already been designed to bind to small G proteins of the Ras superfamily. Ras itself has been targeted with stabilized α-helical peptides that were based on a helix from the exchange factor SOS. Peptides stabilized by the hydrogen bond surrogate method (39) bound to Ras·GDP with a K_d of 160 μM, 10-fold weaker than the catalytic domain of SOS. On the other hand, hydrocarbon-stapled peptides based on the same SOS helix bound to K-Ras with an affinity of around 0.1 μM but were not selective for the GTP-bound form, as expected for a peptide based on an exchange factor (40). Hydrocarbon-stapled peptides based on Rab-binding proteins, including effectors and exchange factors, have been screened against several members of the Rab small G protein family. Several of these bound preferentially to nucleotide-free Rabs, but a K_d of

22 μM was obtained for the most potent stapled peptide with GMPPNP-bound Rab8a, which was also selective for this Rab isoform (50).

We exploited the helical nature of an effector protein in this work to target specifically the GTP-bound form of the Ral proteins, on the basis that this is the form that is downstream of oncogenic Ras and so is active in a disease scenario. We have shown that this is a viable approach, since the highest affinity peptide was indeed specific for the active Ral proteins and showed no interaction with the GDP-bound forms. Can this approach be applied to other small G proteins? For Ras itself it is difficult to envisage, since all the known effectors utilize an intermolecular β-sheet to bind the G protein (reviewed in (34)). Apart from Ras, the largest structural class of effectors for small G proteins is actually those that bind using a helical pair. We have recently classified these into six subclasses, based on their helix orientations, which cover interactions between effectors and members of the Ras, Rho, Arf and Rab families (34). In several cases one of the helices dominates, making the majority of the interactions with the nucleotide-sensitive switch regions and therefore making the relevant small G proteins open to this approach to inhibitor design. Representative examples from 5 of the 6 classes where one helix makes most interactions are: RalB-RLIP76; Arf1-GGA; Rac1-PRK1; Arl1-Arfaptin1 and Arf6-JIP4. Stabilized helical peptides based on effectors may therefore be useful starting points for design of molecules that bind (and inhibit) members of the Arf and Rho families as well as Rab and Ral.

The stapled peptides that we have designed bind to the nucleotide sensitive switch regions of Ral. These regions, as well as being responsible for effector binding, are the sites of interaction with the GEFs and GAPs, the regulators of the G proteins. We tested whether SP1 bound competitively with Ral effectors, and found that it could be fully displaced by RLIP76 and only partially displaced by Sec5. This indicates that SP1 binds to both switch 1 and switch 2. The recent structure of Ral with a GEF protein (Rlf) shows that switch 2 is involved in the GEF interaction and is also important for Ral *vs* Ras selectivity (25). There are currently no structures of Rals in complex with cognate GAPs, but the

RalGAP proteins have closest homology with RapGAPs, and a Rap1b-Rap1GAP complex shows that both switch regions of the Rap protein are involved in the interaction (51). As our peptides do not bind to the GDP-bound form of Ral, they should not compete with GEF proteins for binding but they are likely to bind competitively with the GAP proteins. This implies that they would not prevent Ral proteins being activated (*i.e.* becoming GTP-bound) in the cell but as the peptides would be competitive with GAP binding they could prevent deactivation. Nevertheless, we have demonstrated here the important overall effect of SP1 in cells, which is to prevent Ral signalling by competing with effector binding. Furthermore, GTP-specific peptides would be particularly useful in cells that have reduced RalGAP activity, for example invasive bladder cancer cell lines (27).

Interestingly, we found that RalA·GMPPNP binding to both Peptide 1 and SP1 was of a lower affinity than RalB·GMPPNP binding to the same peptides. The peptides were designed based on the structure of RalB·GMPPNP with RLIP76 RBD. Although the RalA·GMPPNP and RalB·GMPPNP sequences are identical in the regions that bind to RLIP76, mutagenesis of the RLIP76 RBD has revealed some isoform differences (17). Of interest is the observation that mutation of Leu412 in helix α1 to Ala reduces RalA binding 4-fold but does not affect RalB binding. This implies that helix α1 may contribute more to RalA interactions than to RalB binding and raises the exciting prospect that it might be possible to design Ral-isoform specific inhibitors. We also found that the related G protein R-Ras was able to bind to SP1, albeit with a reduced affinity. The binding of R-Ras is not surprising when considering the sequence identity between these two members of the Ras family. Of the 14 residues that contact helix α2 in the structure (Figure 3d and (33)) 11 are identical or represent conservative substitutions in R-Ras. Only Ala48, Arg52 and Ser85 are not conserved in R-Ras. Ala48[RalB] backbone forms a hydrogen bond with the sidechain of Gln433[RLIP76]: the replacement of Ala by Glu in R-Ras should not prevent this directly, although it may alter the conformation of switch 1. Arg52[RalB] forms a hydrogen bond with the backbone of the RLIP76 coiled coil and makes contacts with RLIP76 residues Arg434, Thr437 and Ala438. Replacement of Arg52 by the smaller sidechain of Thr in R-Ras would lead to a rearrangement of these interactions. Finally, Ser85[RalB] forms a hydrogen bond with Glu427[RLIP76]. This would not be able to form when R-Ras binds to RLIP76, because it has an Ala at this position. Therefore the selectivity of SP1 for Ral proteins over R-Ras probably lies in just two residues in Ral, Arg52 and Ser85. These residues also both experience chemical shift changes when SP1 binds and hence contact SP1 directly.

Importantly, SP1 was able to enter mammalian cells, confirming its potential for use as a chemical probe and as a starting point for designing therapeutic peptides. The ability of hydrocarbon staples to enhance cell penetration is perhaps their most important attribute. Several classes of cell penetration enhancement sequences (CPPs) have been identified and successfully employed (52). Enhancement by chemical stapling appears to be due to an increase in the overall hydrophobicity of the peptide as a result of the chemical clamp, and is sequence independent. Cell penetration is likely to be further enhanced by the overall positive charge carried by SP1, as previous studies have suggested that positive charge is often favourable for uptake of constrained peptides into cells (36). A systematic study of more than 200 peptides showed that charges of +1 to +7 are optimal for cellular uptake: as SP1 has a charge of +2 it fits the profile of a peptide that readily enters cells (53). The same study showed that the mechanism of cell uptake of stapled peptides likely involves ATP-dependent endocytosis but is not dependent on calveolin or clathrin. Rather, it may be dependent on anionic cell-surface proteoglycans, explaining the necessity for positive charge.

Our cellular uptake assays indicated that SP1 has a cellular lifetime of at least 16 hours (Figure 6). Furthermore, the activity assays were performed 24 hours after peptide treatment, demonstrating that the peptide was effective for a minimum of 24 hours. Similar activity assays using Peptide 1 revealed some activity in cells after 12 hours, but this had fallen back to the control levels by 24 hours, presumably due to degradation of the unstapled, and therefore unprotected, peptide (data not shown). This is borne out by the lack of signal

11

for FITC-Peptide 1 in cell penetration assays after 16 hours.

Once in cells, SP1 shows clear biological activity. We chose to use inhibition of nutrient starvation-induced autophagocytosis as a cellular readout for peptide activity. RalB, but not RalA, is required for autophagosome biogenesis and is sufficient to activate autophagy. Thus, autophagosome biogenesis is an isoform-specific Ral controlled pathway, which gives a clean readout for inhibition of RalB activity. Our peptides were designed using the RalB-RLIP76 RBD structure and indeed have slightly higher affinity for RalB over RalA. In this assay, clear inhibition by SP1 was achieved at low micromolar concentrations. We also demonstrated the ability of SP1 to inhibit the cellular interaction between RalB and its immediate downstream effector, Sec5 by inhibition of co-immunoprecipitation. We expected that SP1 should be able to interfere with multiple RalB effector interactions, due to the overlap of all known binding sites. RalB activates autophagy via its effector protein, Exo84. The mechanism of action of RalB in autophagy is known to be through initiation of vesicle nucleation, by assembly of the ULK1-Beclin1-VPS34 complex directly on Exo84. Thus inhibition of autophagy suggests that the Exo84 interaction is also inhibited by SP1 in cells. Taken together, the data demonstrate that SP1 inhibits RalB specific pathways via its engineered mode of action by acting as a pan RalB-effector complex inhibitor.

The role of autophagy in cancer has been the subject of much investigation recently. In some contexts autophagy may suppress tumourigenesis but in the majority of situations autophagy is thought to promote tumourigeneis (54). Autophagy is found to be upregulated in Ras-driven cancers and although this seems to be context dependent, autophagy inhibitors may well have utility in defined disease scenarios (55). Thus, the action of our stapled peptides in a cellular pathway important to Ras-driven cancers indicates their utility as both a cellular probe and as a potential therapeutic starting point.

In summary, we have exploited the α-helical nature of the RBD of the Ral effector RLIP76 and

rationally designed stabilized α-helical peptides that bind to Ral proteins and inhibit their interactions with downstream effectors. The constrained peptide displaying the highest affinity for RalB *in vitro* was also capable of entering cells and inhibiting RalB specific cellular functions. Thus this approach represents a potential strategy to interfere with Ras and Ral signalling, as well as providing a chemical tool to investigate Ral function *in vivo*. SP1 binds to Ral and competes with effector proteins, suggesting that it would be able to switch off Ral signalling completely and therefore contribute to the downregulation of oncogenic Ras. Therapeutics against Ras-driven cancers are desperately required; this peptide provides an excellent starting point for development of such a drug that could be used alone or in conjunction with Raf or PI3K inhibitors in a multi-pronged attack on aberrant Ras signalling. These data also provide proof of principle that small G proteins in their active conformation can be targeted using this strategy, which has ramifications for many other small G protein controlled pathways and therefore diseases. Work is ongoing in our laboratories to improve the affinity of the peptide and further explore *in vivo* effects.

Experimental Procedures

Peptide synthesis and characterization

All peptides were synthesized using Fmoc-based solid-phase peptide synthesis (as previously published (44)) on Rink Amide (MBHA) resin (30 μmol scale). Resin was swollen using 1 mL *N*-methyl-2-pyrrolidone (NMP) for 10 min, then Fmoc-deprotection carried out using 2 × 1.5 mL piperidine (25% v/v) in NMP for 10 min, followed by a pair of consecutive dichloromethane (DCM) and NMP washes. Standard amino acid couplings were performed with 800 μL of activated amino acid solution consisting of Fmoc-Xaa-OH (375 μL, 0.4 M, 5 equivalents), PyClock (375 μL, 0.4 M, 5 equivalents) and N,N-diisopropylethylamine (52 μL, 10 equivalents). Each residue was double coupled at room temperature for 2 × 1 h. Unnatural amino acid solutions contained Fmoc-protected amino acid (300 μL, 0.4 M, 4 equivalents), PyClock (300 μL,

0.4 M, 4 equivalents), N,N-diisopropylethylamine (42 μL, 8 equivalents) and were single coupled for 2 h. Peptides containing unnatural amino acids were chemically stapled by reaction with 2 × 1 mL Grubbs' first generation catalyst (6 mM) in 1,2-dichloroethane at room temperature for 2 h. Following the final Fmoc-deprotection, peptide N-termini were acetylated with 2 mL acetylation solution (4% acetic anhydride, 16% N,N-diisopropylethylamine in NMP) for 1 h, or labelled with FITC with 500 μL FITC solution (82 mg FITC (7 equivalents), 73 μL N,N-diisopropylethylamine (14 equivalents) in dimethylformamide (DMF)) overnight. Peptide resins were extensively washed with DCM, methanol and diethylether and dried in a vacuum dessicator overnight, before deprotection using 95% trifluoroacetic acid, 2.5% triisopropylsilane, 2.5% water (1.5 mL) for 2.5 h. Peptides were purified by HPLC and analysed using LCMS and MALDI. The concentrations of stock solutions were checked by amino acid analysis. See Table S1 for characterization data for all peptides synthesized. FAM peptides were purchased from Eurogentec.

Circular dichroism spectroscopy
CD spectra were recorded at 1 nm intervals between 190-260 nm using a Chirascan CD spectrometer with a 1 mm path length quartz cuvette. Three scans were recorded for each peptide, the data averaged and buffer background subtracted. Peptides were measured at 10 μM in 20 mM phosphate buffer, pH 7.5 at 298 K. The helical content of each peptide was determined using CDSSTR, Set 7 and DichroWeb (56).

Protein expression
RalB (residues 1-185, Q72L), RalA (1-184, Q72L), and RLIP76 RBD (residues 393-446, C411S) were expressed and purified as described previously (33,41). Cultures used to express ^{15}N labelled RalB were grown in MOPS minimal media supplemented with [15]NH$_4$Cl, as described previously. All protein tags were cleaved prior to use, as previously described (33). Exchange of nucleotide for GMPPNP was performed as described previously (49). R-Ras (residues 23-201, Q89L) was cloned into pET16b (Novagen) and transformed into BL21(DE3) *E. coli*. Its expression was induced by addition of 1mM IPTG

for 3 hours, and the protein was purified using a Ni-IDA Sepharose column (GE Healthcare) and gel filtration (S75, GE Healthcare).

Isothermal titration calorimetry
ITC data were collected using a MicroCal iTC200 calorimeter at 298 K in 50 mM Tris-HCl, pH 7.5, 1 mM MgCl$_2$. Peptide (1-2 mM) was titrated into protein (70 μM) in 19 × 2 μL additions with 120 s spacing between injections. Control experiments were performed by titrating peptides (1-2 mM) into buffer. Data were fitted using MicroCal Origin 7.0 software using a single-site binding model (N=1). All data shown are representative of at least two independent experiments.

Fluorescence polarization
Fluorescence polarization experiments were measured on a BMG Labtech Pherastar fluorimeter with excitation 485 nm and emission 520 nm at 298 K. Solutions were made up in black, flat-bottomed 384-well plates with 30 μL total volume per well. Ral proteins were serially diluted (doubling dilutions) in 50 mM Tris-HCl, pH 7.5, 100 mM NaCl, 1 mM MgCl$_2$ (maximum final concentration 50 μM) and added to the plate, followed by FITC-peptide (final concentration, 10 nM). Plates were spun at 1000 g for 1 min and then read both immediately and after 30 min incubation at 298 K. Data were fitted to a single-site binding model using non-linear regression analysis in GraphPad Prism 6.0 to obtain K_d values and their standard errors.

Competition fluorescence polarization assays were run as above, using 10 nM FITC-Peptide 5 and 1 μM RalB·GMPPNP in the presence of doubling dilutions of Sec5 or RLIP76 Ral-binding domains (maximum final concentration 30 μM). Data were fitted to a sigmoidal dose-response curve using non-linear regression analysis in GraphPad Prism 6.0 to obtain K_d values and their standard errors.

^{1}H-^{15}N HSQC NMR spectroscopy
Experiments were recorded on a Bruker DRX500 at 298 K using 200 μM ^{15}N-labelled RalB·GMPPNP in 50 mM Tris-HCl, pH 7.5, 50 mM NaCl, 1 mM MgCl$_2$, 10% D$_2$O. For the titration experiments, one, two five and eight equivalents of peptide were added to the protein solution and the spectra recorded after each

13

peptide addition. NMR data were processed using the *AZARA* package (W. Boucher, unpublished) and analyzed using CCPN *ANALYSIS* (57). Overall chemical shift perturbations, δ, were calculated using the equation:

$$\delta = \sqrt{\delta_{1_H}^2 + (0.15\delta_{15_N})^2}$$

where $\delta 1_H$ and $\delta 15_N$ are the chemical shift changes for the ^{1}H and ^{15}N dimensions respectively.

Cellular uptake of peptides

5×10^5 HEK293T cells were seeded into 35 mm glass bottom culture dishes and incubated in 1 mL DMEM supplemented with 10% FBS. After 24 h, FITC alone, FITC-labelled unstapled Peptide 1 or FITC-labelled stapled peptide SP1, were added to a final concentration of 10 µM. After 16 h the cells were fixed in 4% w/v formaldehyde. Images were acquired using a Fluoview 300 Laser scanning confocal microscope with a PLAPON 60X1.42 PLan Apo oil objective and a 60 mm confocal aperture. Cells were excited at 488 nm and emitted light was detected at 510-570 nm. All images were recorded using the same instrument settings.

Co-immunoprecipitation assays

5×10^6 HEK293T cells were seeded 48 h prior to endpoint into 10 cm dishes (3 per condition) in DMEM supplemented with 10% FBS. The medium was aspirated and fresh DMEM (with 10% FBS) with and without FAM-SP1 or SP6 (at 100 µM each) was added 24 h prior to endpoint. The medium was then replaced with 1X EBSS (Earle's Balanced Salt Solution) 90 min prior to endpoint. At endpoint, cells were lysed in lysis buffer (20 mM Tris-HCl pH 7.4, 137 mM NaCl, 1 % Triton X-100, 0.5 % sodium deoxycholate, 10 % Glycerol, 10 mM MgCl$_2$, 2 mM EGTA, 1 mM PMSF, 50 mM NaF, 1 mM NaVO$_4$, 80 mM β-glycerophosphate plus EDTA-free protease inhibitor cocktail (Roche 04693159001)). After 15 min lysis at 4 °C, lysates were cleared at 20,000 g for 20 min at 4 °C. Cell lysates were diluted with lysis buffer to prepare 120 µL of Whole Cell Lysate (WCL) (4 µg/µL) and 1400 µL of IP Lysate (6 µg/µL) for each condition. Endogenous RalB was immunoprecipitated by the addition of 30 µL of mouse anti-RalB antibody (a kind gift from Larry Feig, Tufts University) to IP lysates at 4 °C for 4 h. Protein A/G agarose beads (Santa Cruz Biotechnology Inc., sc-2003) were added for 1 h at 4 °C to precipitate antibody-antigen complexes. Precipitated complexes were washed three times with lysis buffer for 5 min at 4 °C. The samples were then separated via SDS-PAGE and transferred to PVDF membranes (Immobilon-P). Membranes were probed by immunoblotting with the following primary antibodies: rabbit anti-RalB (Cell Signalling Technology cs-3523, lot 1) and mouse anti-Sec5 (a kind gift from Charles Yeaman, University of Iowa).

GFP-LC3 fluorescence quantification and imaging

72 h prior to endpoint, 8×10^3 HeLa cells stably expressing GPF-LC3 were plated per well of glass bottomed 96-well plates. Cells were plated in 100 mL of DMEM supplemented with 10% FBS and grown for 48 h. 24 h prior to endpoint, the medium was changed with 100 mL fresh DMEM (with 10% FBS). DMSO and Peptides were added 24 h prior to endpoint at final indicated concentrations (final concentration of DMSO per well was 1%). 4 h prior to endpoint, cells were washed twice with PBS (with Ca^{2+} and Mg^{2+}) and then fed with either 100 mL of 1X (EBSS) or Serum-Free (SF) DMEM as indicated. At endpoint, EBSS-treated cells were washed once and SF DMEM-treated cells twice with 1X PBS (with Ca^{2+} and Mg^{2+}). Cells were then fixed in 4% PFA in 1X PBS (with Ca^{2+} and Mg^{2+}) for 10 min. Cells were then washed twice as before and then stained with 0.01% Hoechst in 1X PBS (with Ca^{2+} and Mg^{2+}) for 20 min. Total fluorescence intensity for GFP and Hoechst was measured using the PheraStar FS plate-reader. For epifluorescence imaging, HeLa cells stably expressing GPF-LC3 were grown in 384-well plates in DMEM (with 10% FBS) for 48 h. The medium was not changed for DMEM-treated cells and EBSS-treated cells were starved for 2 h prior to live-cell imaging at 20X via the (BD) Pathway 855 High-Content Bioimager.

GFP-TFEB activation

5×10^3 HeLa cells stably expressing GFP-TFEB (48) were plated in 500 µL DMEM (with 10% FBS) per well of 8-Chamber Lab-Tek® II Chambered #1.5 German Coverglass slides and grown overnight. 24 h prior to imaging, the

14

medium was changed with 265 µL fresh DMEM (with 10% FBS) and DMSO or peptides at final concentrations indicated (final concentration of DMSO per well was 1%). 24 h after peptide addition, live-cell images were acquired with an Andor Spinning Disc Confocal Microscope (oil immersion and 60X objective) under normal cell culture conditions (37 ^{0}C, 5% CO_2). Initial images of fed-state cells were taken 24 h after peptide addition. The medium in each well was then changed with 265 µL 1 X EBSS and subsequent images were taken at the times indicated above.

Conflict of Interest
The authors declare that they have no conflicts of interest with the contents of this article. The content is solely the responsibility of the authors and does not necessarily represent the official views of the National Institutes of Health.

Author Contributions
JCT synthesized all peptides and performed all biophysical and structural analyses. HRM performed NMR experiments and data processing. NSC and DO undertook the cell penetration experiments. JC and CW performed the co-immunoprecipitation and autophagy assays. MAW oversaw all cell biology. CA oversaw all chemistry. DO and HRM directed all aspects of the overall project. JCT, HRM and DO wrote the manuscript. All co-authors participated in discussions and in editing the final manuscript.

References

1.   Stephen, A. G., Esposito, D., Bagni, R. K., and McCormick, F. (2014) Dragging Ras back in the ring. *Cancer Cell* **25**, 272-281
2.   Jones, S., and Thornton, J. M. (1996) Principles of protein-protein interactions. *Proc. Natl. Acad. Sci. U. S. A.* **93**, 13-20
3.   Arkin, M. R., and Wells, J. A. (2004) Small-molecule inhibitors of protein-protein interactions: progressing towards the dream. *Nat. Rev. Drug Discov.* **3**, 301-317
4.   Arkin, M. R., Tang, Y., and Wells, J. A. (2014) Small-molecule inhibitors of protein-protein interactions: progressing toward the reality. *Chem. Biol.* **21**, 1102-1114
5.   Gysin, S., Salt, M., Young, A., and McCormick, F. (2011) Therapeutic strategies for targeting Ras proteins. *Genes Cancer* **2**, 359-372
6.   Cox, A. D., Fesik, S. W., Kimmelman, A. C., Luo, J., and Der, C. J. (2014) Drugging the undruggable RAS: mission possible? *Nat. Rev. Drug Discov.* **13**, 828-851
7.   Fiordalisi, J. J., Johnson, R. L., Weinbaum, C. A., Sakabe, K., Chen, Z., Casey, P. J., and Cox, A. D. (2003) High affinity for farnesyltransferase and alternative prenylation contribute individually to K-Ras4B resistance to farnesyltransferase inhibitors. *J. Biol. Chem.* **278**, 41718-41727
8.   Ostrem, J. M., Peters, U., Sos, M. L., Wells, J. A., and Shokat, K. M. (2013) K-Ras(G12C) inhibitors allosterically control GTP affinity and effector interactions. *Nature* **503**, 548-551
9.   Baines, A. T., Xu, D., and Der, C. J. (2011) Inhibition of Ras for cancer treatment: the search continues. *Future Med. Chem.* **3**, 1787-1808

10.   Holderfield, M., Deuker, M. M., McCormick, F., and McMahon, M. (2014) Targeting RAF kinases for cancer therapy: BRAF-mutated melanoma and beyond. *Nat. Rev. Cancer* **14**, 455-467

11.   Fruman, D. A., and Rommel, C. (2014) PI3K and cancer: lessons, challenges and opportunities. *Nat. Rev. Drug Discov.* **13**, 140-156

12.   Bodemann, B. O., and White, M. A. (2008) Ral GTPases and cancer: linchpin support of the tumorigenic platform. *Nat. Rev. Cancer* **8**, 133-140

13.   Neel, N. F., Martin, T.D., Stratford, J.K., Zand, T.P., Reiner, D.J. and Der, C.J. (2011) The RalGEF-Ral effector signaling network: the road less traveled for anti-Ras drug discovery. *Genes Cancer* **2**, 275–287

14.   Moskalenko, S., Henry, D. O., Rosse, C., Mirey, G., Camonis, J. H., and White, M. A. (2002) The exocyst is a Ral effector complex. *Nat. Cell Biol.* **4**, 66-72

15.   Sugihara, K., Asano, S., Tanaka, K., Iwamatsu, A., Okawa, K., and Ohta, Y. (2002) The exocyst complex binds the small GTPase RaIA to mediate filopodia formation. *Nat. Cell Biol.* **4**, 73-78

16.   Chien, Y. C., Kim, S., Bumeister, R., Loo, Y. M., Kwon, S. W., Johnson, C. L., Balakireva, M. G., Romeo, Y., Kopelovich, L., Gale, M., Yeaman, C., Camonis, J. H., Zhao, Y. M., and White, M. A. (2006) RaIB GTPase-mediated activation of the I kappa B family kinase TBK1 couples innate immune signaling to tumor cell survival. *Cell* **127**, 157-170

17.   Campbell, L., Peppa, M., Crabtree, M., Shafiq, A., McGough, N., Mott, H.R. and Owen, D. (2015) Thermodynamic mapping of effector protein interfaces with RalA and RalB. *Biochemistry* **54**, 1380-1389

18.   Fukai, S., Matern, H. T., Jagath, J. R., Scheller, R. H., and Brunger, A. T. (2003) Structural basis of the interaction between RalA and Sec5, a subunit of the sec6/8 complex. *EMBO J.* **22**, 3267

19.   Jin, R. S., Junutula, J. R., Matern, H. T., Ervin, K. E., Scheller, R. H., and Brunger, A. T. (2005) Exo84 and Sec5 are competitive regulatory Sec6/8 effectors to the RalA GTPase. *EMBO J.* **24**, 2064-2074

20.   Shipitsin, M., and Feig, L. A. (2004) RalA but not RalB enhances polarized delivery of membrane proteins to the basolateral surface of epithelial cells. *Mol. Cell. Biol.* **24**, 5746-5756

21.   Lim, K.-H., Brady, D. C., Kashatus, D. F., Ancrile, B. B., Der, C. J., Cox, A. D., and Counter, C. M. (2010) Aurora-A phosphorylates, activates, and relocalizes the small GTPase RalA. *Mol. Cell. Biol.* **30**, 508-523

22.   Wang, H., Owens, C., Chandra, N., Conaway, M. R., Brautigan, D. L., and Theodorescu, D. (2010) Phosphorylation of RalB is important for bladder cancer cell growth and metastasis. *Cancer Res.* **70**, 8760-8769

23.   Martin, T. D., Mitin, N., Cox, A. D., Yeh, J. J., and Der, C. J. (2012) Phosphorylation by protein kinase C alpha regulates RalB small GTPase protein activation, subcellular localization, and effector utilization. *J. Biol. Chem.* **287**, 14827-14836

24.   Neyraud, V., Aushev, V. N., Hatzoglou, A., Meunier, B., Cascone, I., and Camonis, J. (2012) RalA and RalB proteins are ubiquitinated GTPases, and ubiquitinated RalA increases lipid raft exposure at the plasma membrane. *J. Biol. Chem.* **287**, 29397-29405

25.   Popovic, M., Schouten, A., Rensen-de Leeuw, M., and Rehmann, H. (2016) The structure of the guanine nucleotide exchange Factor Rlf in complex with the small G-protein Ral identifies conformational intermediates of the exchange reaction and the basis for the selectivity. *J. Struct. Biol.* **193**, 106-114

26.   Shirakawa, R., Fukai, S., Kawato, M., Higashi, T., Kondo, H., Ikeda, T., Nakayama, E., Okawa, K., Nureki, O., Kimura, T., Kita, T., and Horiuchi, H. (2009) Tuberous sclerosis tumor suppressor complex-like complexes act as GTPase-activating proteins for Ral GTPases. *J. Biol. Chem.* **284**, 21580-21588

27.   Saito, R., Shirakawa, R., Nishiyama, H., Kobayashi, T., Kawato, M., Kanno, T., Nishizawa, K., Matsui, Y., Ohbayashi, T., Horiguchi, M., Nakamura, T., Ikeda, T., Yamane, K., Nakayama, E., Nakamura, E., Toda, Y., Kimura, T., Kita, T., Ogawa, O., and Horiuchi, H. (2013)

Downregulation of Ral GTPase-activating protein promotes tumor invasion and metastasis of bladder cancer. *Oncogene* **32**, 894-902

28.   Chien, Y. C., and White, M. A. (2003) RAL GTPases are linchpin modulators of human tumour-cell proliferation and survival. *EMBO Reports* **4**, 800-806

29.   Lim, K. H., Baines, A. T., Fiordalisi, J. J., Shipitsin, M., Feig, L. A., Cox, A. D., Der, C. J., and Counter, C. M. (2005) Activation of RaIA is critical for Ras-induced tumorigenesis of human cells. *Cancer Cell* **7**, 533

30.   Lim, K.-H., O'Hayer, K., Adam, S. J., Kendall, S. D., Campbell, P. M., Der, C. J., and Counter, C. M. (2006) Divergent roles for RalA and RalB in malignant growth of human pancreatic carcinoma cells. *Curr. Biol.* **16**, 2385-2394

31.   Martin, T. D., and Der, C. J. (2012) Differential involvement of RalA and RalB in colorectal cancer. *Small GTPases* **3**, 126-130

32.   Yan, C., Liu, D., Li, L., Wempe, M. F., Guin, S., Khanna, M., Meier, J., Hoffman, B., Owens, C., Wysoczynski, C. L., Nitz, M. D., Knabe, W. E., Ahmed, M., Brautigan, D. L., Paschal, B. M., Schwartz, M. A., Jones, D. N. M., Ross, D., Meroueh, S. O., and Theodorescu, D. (2014) Discovery and characterization of small molecules that target the GTPase Ral. *Nature* **515**, 443-447

33.   Fenwick, R. B., Campbell, L. J., Rajasekar, K., Prasannan, S., Nietlispach, D., Camonis, J., Owen, D., and Mott, H. R. (2010) The RaIB-RLIP76 complex reveals a novel mode of RaI-effector interaction. *Structure* **18**, 985-995

34.   Mott, H. R. and Owen, D. (2015) Structures of Ras superfamily effector complexes: What have we learnt in two decades? *Crit. Rev. Biochem. Mol. Biol.* **50**, 85-133

35.   Bodemann, B. O., Orvedahl, A., Cheng, T., Ram, R. R., Ou, Y.-H., Formstecher, E., Maiti, M., Hazelett, C. C., Wauson, E. M., Balakireva, M., Camonis, J. H., Yeaman, C., Levine, B., and White, M. A. (2011) RalB and the exocyst mediate the cellular starvation response by direct activation of autophagosome assembly. *Cell* **144**, 253-267

36.   Walensky, L. D., and Bird, G. H. (2014) Hydrocarbon-stapled peptides: principles, practice, and progress. *J. Med. Chem.* **57**, 6275-6288

37.   Wittrup, K. D., and Verdine, G. L. (2012) Protein engineering for therapeutics, Part A. Preface. *Methods Enzymol.* **502**, xiii-xiv

38.   Aileron. (2013, 2015) Aileron therapeutics successfully completes stapled peptide Phase 1 clinical trials. Aileron Therapeutics Initiates Phase 1 Cancer Study of ALRN-6924 in Advanced Hematologic and Solid Malignancies with Wild Type p53. in *News Release*, http://aileronrx.com/index.php

39.   Patgiri, A., Yadav, K. K., Arora, P. S., and Bar-Sagi, D. (2011) An orthosteric inhibitor of the Ras-Sos interaction. *Nat. Chem. Biol.* **7**, 585-587

40.   Leshchiner, E. S., Parkhitko, A., Bird, G. H., Luccarelli, J., Bellairs, J. A., Escudero, S., Opoku-Nsiah, K., Godes, M., Perrimon, N., and Walensky, L. D. (2015) Direct inhibition of oncogenic KRAS by hydrocarbon-stapled SOS1 helices. *Proc. Natl. Acad. Sci. U. S. A.* **112**, 1761-1766

41.   Prasannan, S., Fenwick, R.B., Campbell, L.J., Evetts, K.A., Nietlispach, D., Owen, D. and Mott, H.R. (2007) 1H, 13C, and 15N resonance assignments for the small G protein RalB in its active conformation. *Biomol. NMR Assign.* **1**, 147-149

42.   Fenwick, R. B., Prasannan, S., Campbell, L. J., Nietlispach, D., Evetts, K. A., Camonis, J., Mott, H. R., and Owen, D. (2009) Solution structure and dynamics of the small GTPase RalB in its active conformation: significance for effector protein binding. *Biochemistry* **48**, 2192-2206

43.   Hubbard, S. J., and Thornton, J.M. (1993) NACCESS. Department of Biochemistry and Molecular Biology, University College London

44.   Kim, Y.-W., Grossmann, T. N., and Verdine, G. L. (2011) Synthesis of all-hydrocarbon stapled alpha-helical peptides by ring-closing olefin metathesis. *Nat. Protoc.* **6**, 761-771

45. Moellering, R. E., Cornejo, M., Davis, T. N., Del Bianco, C., Aster, J. C., Blacklow, S. C., Kung, A. L., Gilliland, D. G., Verdine, G. L., and Bradner, J. E. (2009) Direct inhibition of the NOTCH transcription factor complex. *Nature* **462**, 182-U157

46. Grossmann, T. N., Yeh, J. T. H., Bowman, B. R., Chu, Q., Moellering, R. E., and Verdine, G. L. (2012) Inhibition of oncogenic Wnt signaling through direct targeting of beta-catenin. *Proc. Natl. Acad. Sci. U. S. A.* **109**, 17942-17947

47. Pena-Llopis, S., Vega-Rubin-de-Celis, S., Schwartz, J. C., Wolff, N. C., Tran, T. A. T., Zou, L., Xie, X.-J., Corey, D. R., and Brugarolas, J. (2011) Regulation of TFEB and V-ATPases by mTORC1. *EMBO J.* **30**, 3242-3258

48. Roczniak-Ferguson, A., Petit, C. S., Froehlich, F., Qian, S., Ky, J., Angarola, B., Walther, T. C., and Ferguson, S. M. (2012) The transcription factor TFEB links mTORC1 signaling to transcriptional control of lysosome homeostasis. *Sci. Sig.* **5**, ra42

49. Thompson, G., Owen, D., Chalk, P. A., and Lowe, P. N. (1998) Delineation of the Cdc42/Rac-binding domain of p21-activated kinase. *Biochemistry* **37**, 7885-7891

50. Spiegel, J., Cromm, P. M., Itzen, A., Goody, R. S., Grossmann, T. N., and Waldmann, H. (2014) Direct targeting of Rab-GTPase-effector interactions. *Angew. Chem. Int. Ed.* **53**, 2498-2503

51. Scrima, A., Thomas, C., Deaconescu, D., and Wittinghofer, A. (2008) The Rap-RapGAP complex: GTP hydrolysis without catalytic glutamine and arginine residues. *EMBO J.* **27**, 1145-1153

52. Kauffman, W. B., Fuselier, T., He, J., and Wimley, W. C. (2015) Mechanism matters: a taxonomy of cell penetrating peptides. *Trends Biochem. Sci.* **40**, 749-764

53. Chu, Q., Moellering, R. E., Hilinski, G. J., Kim, Y.-W., Grossmann, T. N., Yeh, J. T. H., and Verdine, G. L. (2015) Towards understanding cell penetration by stapled peptides. *Med. Chem. Comm* **6**, 111-119

54. Yang, Z. J., Chee, C. E., Huang, S., and Sinicrope, F. A. (2011) The role of autophagy in cancer: therapeutic implications. *Mol. Cancer Ther.* **10**, 1533-1541

55. White, E. (2015) The role for autophagy in cancer. *J. Clin. Invest.* **125**, 42-46

56. Whitmore, L., and Wallace, B. A. (2004) DICHROWEB, an online server for protein secondary structure analyses from circular dichroism spectroscopic data. *Nucleic Acids Res.* **32**, W668-W673

57. Vranken, W. F., Boucher, W., Stevens, T. J., Fogh, R. H., Pajon, A., Llinas, P., Ulrich, E. L., Markley, J. L., Ionides, J., and Laue, E. D. (2005) The CCPN data model for NMR spectroscopy: development of a software pipeline. *Proteins: Struct. Funct. Bioinf.* **59**, 687-696

Footnotes.
[1]The abbreviations used are:

GEF – guanine nucleotide exchange factor; GAP – GTPase activating protein; PI3K – phosphoinositide 3-kinase; RBD – Ral-binding domain; FITC – fluorescein isothiocyanate; NMP – N-methyl-2-pyrrolidone; LCMS – liquid chromatography mass spectrometry; MALDI – matrix assisted laser desorption/ionization; CD – circular dichroism; MOPS – (3-(N-morpholino)propanesulphonic acid; ITC – isothermal titration calorimetry; FP – fluorescence polarization; HSQC – heteronuclear single quantum correlation; DMEM – Dulbecco's modified Eagle's medium; FBS – foetal bovine serum; EBSS – Earle's balanced salt solution; PMSF – phenylmethane sulphonyl fluoride; LC3 – microtubule-associated protein 1A/1B-light chain 3 (LC3); PFA – paraformaldehyde; ULK1 – Unc-51 like autophagy activating kinase 1.

Figure legends

Figure 1: Design and synthesis of RLIP76-based peptides. (a) The structure of the RLIP76 RBD bound to RalB·GMPPNP (pdb: 2KWI) revealed key binding residues. RalB is coloured blue and the two switch regions are labelled. RLIP76 is coloured as follows: the segment of the N-terminal helix that contacts RalB is coloured green, the rest of the N-terminal helix is grey, the C-terminal helix is coloured pink and the sidechains of residues whose mutation reduced the binding to RalB more than 5-fold (17) are coloured yellow. The peptides synthesized are shown schematically, with the same colour coding and the staple represented as a single i, i+4 olefin link. (b) CD spectra of the RLIP76 RBD and the peptides generated in this study. (c) Sequences of the peptides used in this study and helicity calculated from analysis of CD data of the RLIP76 RBD and the peptides. Several peptides were synthesized containing all-hydrocarbon staples of various lengths in different positions (indicated by X). Peptides 1 and SP1-SP5 were based on the sequence of the second RLIP76 RBD α-helix sequence; Peptides 2 and SP6 were based on the first α-helix. The α-helicity of the peptides assessed using CD spectroscopy confirmed that several of the stapled peptides synthesized are more helical than the unstapled version of the peptide.

Figure 2. Peptides corresponding to helix α2 are sufficient to bind to Ral proteins. Representative data from ITC experiments are shown for titrations of: (a) the RLIP76 RBD into RalB·GMPPNP; (b) Peptide 1 into RalB·GMPPNP; (c) Peptide 2 into RalB·GMPPNP; (d) Peptide 1 into RalA·GMPPNP; (e) Peptide 1 into Rac1·GMPPNP. The parameters for the fit for these individual experiments are shown in each panel. For the average parameters obtained from several experiments, see Table 1.

Figure 3: Peptide 1 binds to RalB in an analogous manner to RLIP76 RBD. (a) Section of ^{1}H-^{15}N HSQC NMR spectra of ^{15}N RalB·GMPPNP alone (blue) and in the presence of excess Peptide 1 (red) or RLIP76 RBD (black). Addition of Peptide 1 caused the movement of several peaks, all of which also shifted upon the addition of RLIP76 RBD. The changes in crosspeaks when Peptide 1 is added to RalB are smaller than those observed when RLIP76 RBD is added but the peaks shift in the same direction (see dotted lines *e.g.* Lys16, Val20, Lys27, Tyr51, Arg52). Peaks that do not shift when RLIP76 RBD is added (*e.g.* Asn128) do not shift when Peptide 1 is added. (b) The chemical shift changes were plotted for each residue of RalB. The secondary structural elements are shown above the graph, where β-strands are represented by arrows and α-helices by cylinders. Red lines indicate the locations of the two switch regions. The dashed blue line shows the position of the average chemical shift change (0.047) and the solid green line shows the standard deviation of the chemical shift changes (0.068) (c) RalB residues that shifted by more than one standard deviation upon titration of Peptide 1 are highlighted on the structure of RalB·GMPPNP (blue) and show that Peptide 1 binds to RalB in the same place as RLIP76 RBD α2 (shown in pink). Residues that are shifted but which are more than 50% buried are shown as yellow sticks. Residues that are shifted but are solvent exposed are shown as orange spheres and are identified with a label. (d) Sequence alignment of RalA/B and R-Ras in the region that interacts with RLIP76 RBD. RalA and RalB have identical sequences in this region. Residue conservation is denoted below the alignment: * = identical, : = conservative substitution. Ral residues surrounded by a grey box interact with the N-terminal helix of RLIP76 RBD (helix α1); residues coloured magenta interact with the C-terminal helix of RLIP76 RBD (helix α2). The symbols above the RalA/B sequence denote residues that form hydrogen bonds or salt bridges involving backbone (+) or sidechain (*) atoms of RalB. The symbols are coloured grey for RLIP76 RBD α1 interactions and magenta for α2 interactions. Red lines indicate the locations of the two switch regions.

Figure 4: Peptide stapling can increase affinity of RalB binding. ITC data for stapled peptides titrated into RalB·GMPPNP at 298 K (a) SP1; (b) SP2; (c) SP3; (d) SP4; (e) SP5 and (f) SP6. The parameters for the fit for the individual experiments are shown. For a summary of the parameters from several

19

experiments, see Table 1. SP5 could not be accurately fit, although the heat changes observed indicate that the peptide does bind. A lower limit on the K_d is given but no reliable parameters can be obtained.

Figure 5. FITC-SP1 binding to Ral is specific, GTP dependent and competitive with Ral effectors.
(a) Fluorescence polarization assays using FITC labelled SP1 confirm that SP1 binds RalB (K_d 5.6 ± 0.3 μM, solid line). SP1 also binds weakly to R-Ras (K_d 30.0 ± 18.0 μM, dashed line); (b) Peptide 1 binds weakly to RalB and even less tightly to R-Ras. Affinity was too low for reliable fitting; (c) SP1 binds RalA·GMPPNP with similar affinity to RalB·GMPPNP (K_d 14.2 ± 8.2 μM, solid line) but does not show significant binding to RalA·GDP (dashed line); (d) Competition fluorescence polarization assays showed that both RLIP76 (solid line) and Sec5 (dashed line) displaced FITC-SP1 from RalB, suggesting FITC-SP1 binds to RalB on an overlapping surface. Data were fitted to give IC$_{50}$ 8.2 ± 2.6μM (Sec5 RBD) and IC$_{50}$ 2.0 ± 1.2μM (RLIP76 RBD). All FP experiments were performed in duplicate and error bars show the standard deviation of the duplicates.

Figure 6: FITC-SP1 can enter mammalian cells and inhibits the interaction between RalB and Sec5.
(a) Wide-field image and (b) single-cell image of HEK293T cells treated with 10 μM FITC-Peptide1, 10 μM FITC-SP1 or 10 μM FITC control overnight. Chemical stapling enables FITC-SP1 to penetrate the cell membrane and localize in both the cytosol and nucleus; (c) SP1 disrupts RalB-Sec5 interaction in cells. HEK293T cells were treated for 24 h with SP1 and SP6 as indicated. The numbers above the Western blot represent the relative intensities of the Sec5 band, normalized to the no-peptide control. Endogenous RalB was immunoprecipitated with mouse anti-RalB antibody. Immunoblotting was conducted with primary antibodies against RalB and Sec5. * marks the band specific to Sec5. Ab, mouse anti-RalB antibody alone. WCL, Whole Cell Lysate.

Figure 7: SP1 can prevent RalB-driven autophagosome assembly in HeLa cells. (a) RalB-Exo84 dependent autophagy (b) epifluorescent images of GFP-LC3 in HeLa cells stably expressing GFP-LC3. Diffuse and punctate GFP-LC3 fluorescence (left panel) is quickly quenched upon recruitment to maturing autophagolysosomes (right panel) (c) quantitation of total GFP-LC3 fluorescence/cell detected under the indicated treatment conditions. Values represent population-based fluorescence-intensity ratios of GFP-LC3:Hoechst stain following 24 h pretreatment with peptides in GFP-LC3 HeLa cells. Error bars indicate standard deviation from the mean, N=4 (d) Subcellular distribution of GFP-TFEB fusion protein was monitored under the indicated conditions in HeLa cells stably expressing GFP-TFEB. Cells were treated with 20 μM SP1 and SP6. Images are representative of multiple fields of view.

Table 1. Summary of binding parameters obtained from ITC for RLIP76 and peptides titrated into Ral proteins. The value obtained from an orthogonal assay, FP, is included for the tightest binding peptide.

Binding partners	K_d (µM)	ΔH (kcal mol^{-1})	TΔS (kcal mol^{-1})	N[a]
RalB·GMPPNP + RLIP76 RBD (n = 2[b])	1.9 ± 0.07[c]	-17.5 ± 1.8	-9.6 ± 1.8	0.9
RalB·GMPPNP + Peptide 1 (n = 4)	29.8 ± 7.3	-1.6 ± 0.6	4.6 ± 0.7	1.1
RalA·GMPPNP + Peptide 1 (n = 3)	43.0 ± 10.8	-1.8 ± 0.9	4.2 ± 0.9	1.0
RalB·GMPPNP + SP1 (n = 3)	4.7 ± 1.6 (5.6 ± 0.3[d])	-0.7 ± 0.4	6.6 ± 0.2	1.0
RalB·GMPPNP + SP2 (n = 2)	10.3 ± 2.3	-0.8 ± 0.0	6.0 ± 0.1	1.1
RalB·GMPPNP + SP3 (n = 3)	53.3 ± 17.8	-0.7 ± 0.3	5.1 ± 0.5	0.9
RalB·GMPPNP + SP4[e]	50.8	-0.4	5.5	1.0
RalB·GMPPNP + SP5 (n = 3)	>24	Not fitted	Not fitted	Not fitted

[a] Stoichiometry

[b] number of experiments

[c] standard deviation of value obtained from multiple experiments

[d] value obtained from FP

[e] Peptide behaved poorly in assays and showed low heat changes: data from a single experiment only
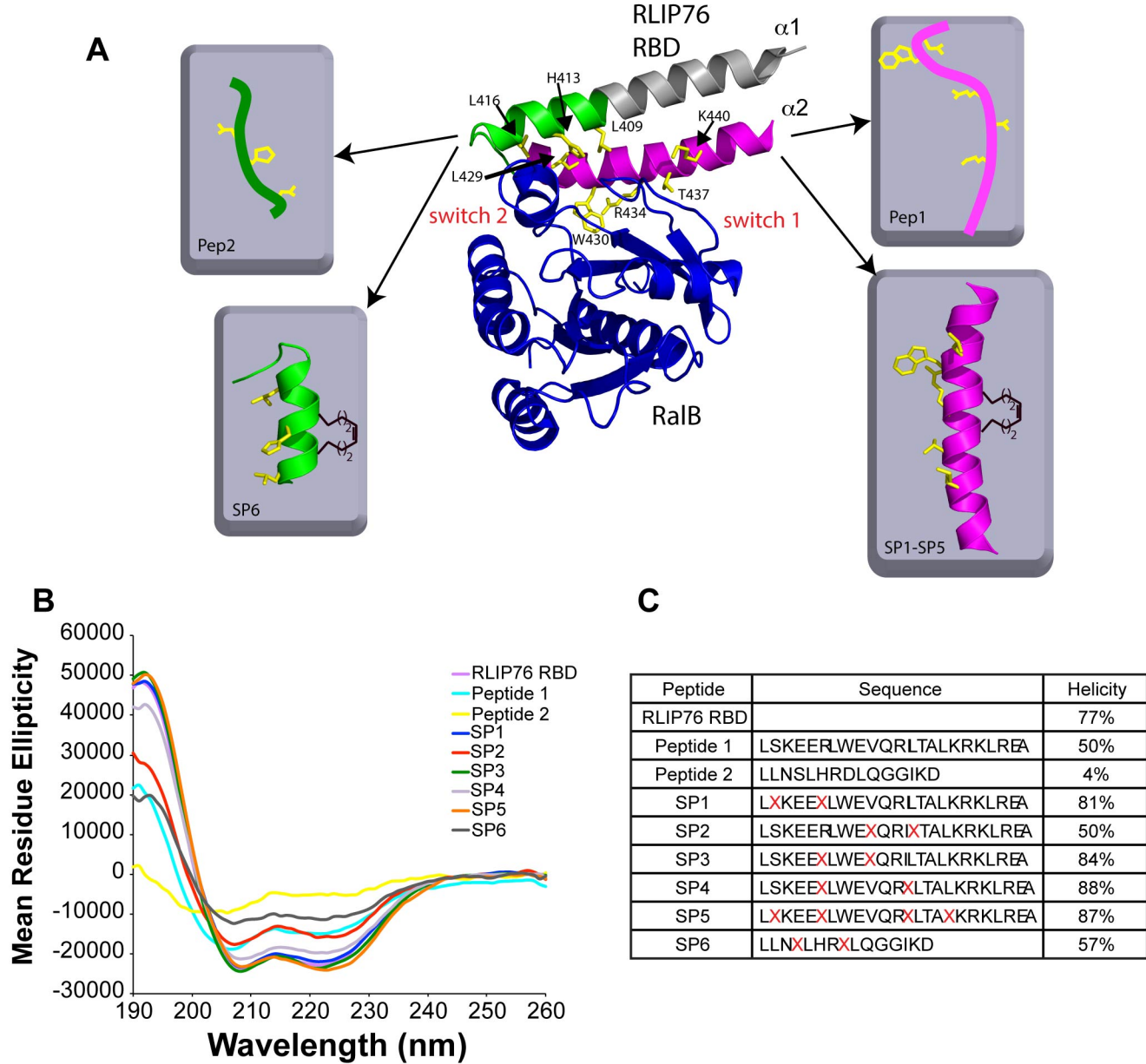
A

RLIP76 RBD

α1

H413
L416
L409
K440
α2

L429
switch 2
R434
T437
W430
switch 1

RalB

Pep2

Pep1

SP6

SP1-SP5

B

- RLIP76 RBD
- Peptide 1
- Peptide 2
- SP1
- SP2
- SP3
- SP4
- SP5
- SP6

C

Peptide	Sequence	Helicity
RLIP76 RBD		77%
Peptide 1	LSKEERLWEVQRLTALKRKLREA	50%
Peptide 2	LLNSLHRDLQGGIKD	4%
SP1	LXKEEXLWEVQRLTALKRKLREA	81%
SP2	LSKEERLWEXQRIXTALKRKLREA	50%
SP3	LSKEEXLWEXQRILTALKRKLREA	84%
SP4	LSKEEXLWEVQRXLTALKRKLREA	88%
SP5	LXKEEXLWEVQRXLTAXKRKLREA	87%
SP6	LLNXLHRXLQGGIKD	57%

Figure 1

Figure 2

A

RalB alone
RalB + Peptide 1
RalB + RLIP76 RBD

B

sw1
sw2

Chemical Shift Perturbatio

Residue Number

C

N-terminal helix

C-terminal helix

Asn81

Ser85

Ile78

Arg52

Asp49

Val40

Glu41

Tyr36

D

```
15                        38
  HKVIMVGSGGVGKSALTLQFMYDE   RalA/B
  HKLVVVGGGGVGKSALTIQFIQSY   R-Ras
30                        53
  * *::  **  *********:**:
```

sw1

```
      + *+ * *
39                        62
  FVEDYEPTK ADSYR KKVVLDGEEV   RalA/B
  FVSDYDPTIEDSYTKICSVDGIPA   R-Ras
54                        77
  **   **:**   *** *   :**
```

sw2

```
                        ++
   *           +        ** **
63                        86
  QIDILDTAGQE DYA AIRD NY FRSG   RalA/B
  RLDILDTAGQEEFGAMREQYMRAG   R-Ras
78                       101
  :: ********** :  *:*::*:*:*
```

Figure 3

Figure 4

A RalB·GMPPNP + SP1
$K_d = 3.1 \pm 1.5$ μM
N = 1.0 ± 0.04
ΔH = -1.0 ± 0.06 kcal/mol
TΔS = 6.5 kcal/mol

B RalB·GMPPNP + SP2
$K_d = 12.4 \pm 2.0$ μM
N = 1.1 ± 0.03
ΔH = -0.8 ± 0.04 kcal/mol
TΔS = 5.9 kcal/mol

C RalB·GMPPNP + SP3
$K_d = 57.1 \pm 13.8$ μM
N = 0.9 ± 0.2
ΔH = -1.1 ± 0.02 kcal/mol
TΔS = 4.7 kcal/mol

D RalB·GMPPNP + SP4
$K_d = 50.8 \pm 21.6$ μM
N = 1.0 ± 0.3
ΔH = -0.36 ± 0.1 kcal/mol
TΔS = 5.5 kcal/mol

E RalB·GMPPNP + SP5
$K_d > 24$ μM

F RalB·GMPPNP + SP6
No heat changes

A

FITC-SP1

B

FITC-Peptide 1

C

D

Figure 5

A

	Bright field	FITC	Overlay
FITC			
FITC-Pep1			
FITC-SP1			

B

	Bright field	FITC	Overlay
FITC			
FITC-Pep1			
FITC-SP1			

C

- SP1 SP6 : Stapled Peptide
1.0 0.1 0.4

100 kDa -
*
75 kDa -
: Sec5

25 kDa -
: RalB

Ab   IP: RalB

100 kDa - - Sec5

25 kDa - - RalB

WCL

Figure 6

A AUTOPHAGY

RalB — Exo84

LC3II Recruited

LC3II

Phagophore → Fusion with Lysosome → Autophagolysosome

Lysosome

LC3II Degraded

B

DMEM   EBSS

GFP-LC3 HeLa

Figure 7

C

DMEM-H (Serum Free) 4hrs   EBSS 4hrs

Ratio GFP/Hoechst

Cells only, DMSO, SP6 (1µM), SP6 (5µM), SP6 (20µM), SP6 (100µM), SP1 (1µM), SP1 (5µM), SP1 (20µM), SP1 (100 µM), Cells only, DMSO, SP6 (1µM), SP6 (5µM), SP6 (20µM), SP6 (100µM), SP1 (1µM), SP1 (5µM), SP1 (20µM), SP1 (100 µM)

D

Pre-fed   EBSS 30min   EBSS 60min   EBSS 90min

DMSO

SP6 – 20µM

SP1 – 20µM

GFP-TFEB HeLa
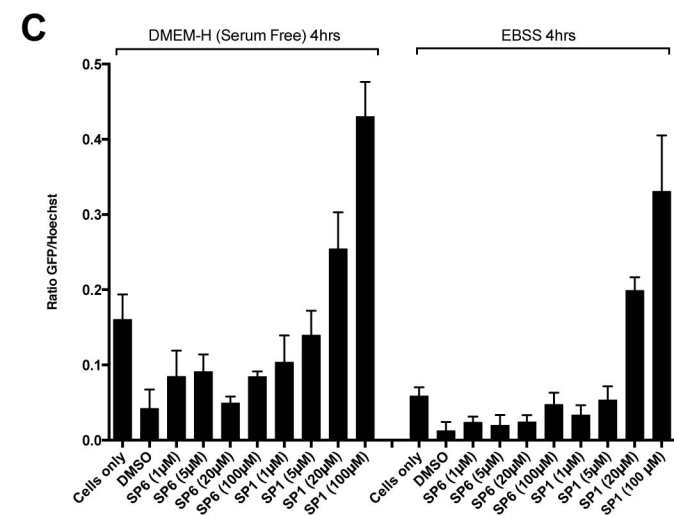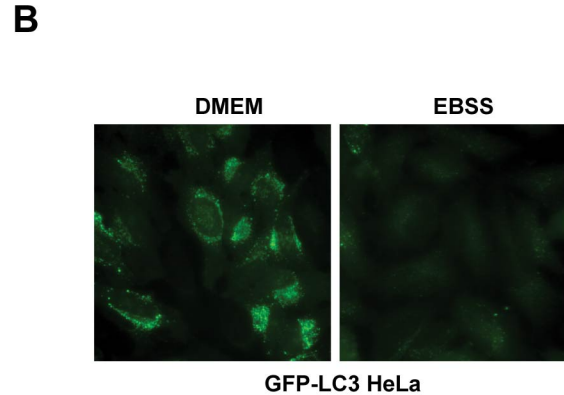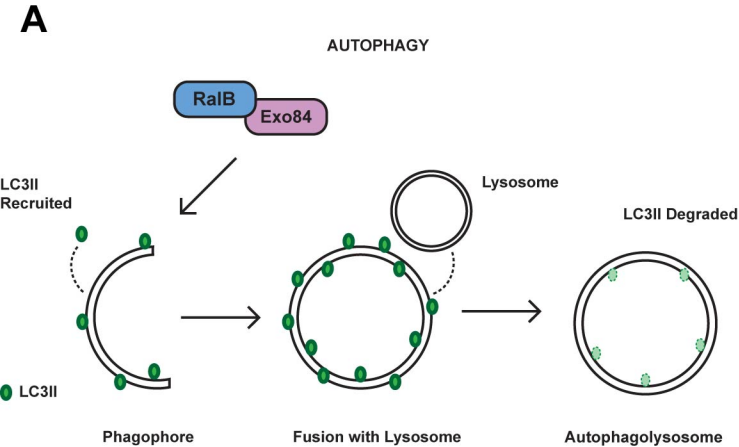
Inhibition of Ral GTPases using a stapled peptide approach

Jemima C. Thomas1,2,4, Jonathan M. Cooper3, Natasha S. Clayton1, Chensu Wang3, Michael A. White3, Chris Abell2, Darerca Owen1* and Helen R. Mott1*

	Sequence	R_t (min)	Calculated MW $[M+H]^+$	Observed MW $[M+H]^+$
Peptide 1	LSKEERLWEVQRILTALKRKLREA	13.3	3006	3006
Peptide 2	LLNSLHRDLQGGIKD	12.3	1719	1719
SP1	L**X**KEE**X**LWEVQRILTALKRKLREA	16.9	3041	3041
SP2	LSKEERLWE**X**QRI**X**TALKRKLREA	19.5	3045	3044
SP3	LSKEE**X**LWE**X**QRILTALKRKLREA	15.6	3029	3029
SP4	LSKEE**X**LWEVQR**X**LTALKRKLREA	16.0	3057	3057
SP5	L**X**KEE**X**LWEVQR**X**LTA**X**KRKLREA	16.6	3093	3093
SP6	LLN**X**LHR**X**LQGGIKD	17.0	1796	1796
FITC-Peptide 1	FITC-$^\beta$ALSKEERLWEVQRILTALKRKLREA	14.7	3427	1714 (m/2), 1143 (m/3)
FITC-SP1	FITC-$^\beta$AL**X**KEE**X**LWEVQRILTALKRKLREA	19.8	3433	1144 (m/3), 859 (m/4)

Table S1: Characterization data for all peptides synthesised.

Inhibition of Ral GTPases Using a Stapled Peptide Approach

Jemima C. Thomas, Jonathan M. Cooper, Natasha S. Clayton, Chensu Wang, Michael A. White, Chris Abell, Darerca Owen and Helen R. Mott

___

Access the most updated version of this article at doi: 10.1074/jbc.M116.720243

Alerts:
- When this article is cited
- When a correction for this article is posted

Click here to choose from all of JBC's e-mail alerts

Supplemental material:
http://www.jbc.org/content/suppl/2016/06/22/M116.720243.DC1.html

This article cites 0 references, 0 of which can be accessed free at
http://www.jbc.org/content/early/2016/06/22/jbc.M116.720243.full.html#ref-list-1